Dynamic Article Links ▶

PAPER

The anisotropic effect of functional groups in ¹H NMR spectra is the molecular response property of spatial nucleus independent chemical shifts (NICS)—Conformational equilibria of *exo/endo* tetrahydrodicyclopentadiene derivatives

Erich Kleinpeter,* Anica Lämmermann and Heiner Kühn

The inversion of the flexible five-membered ring in tetrahydrodicyclopentadiene (TH-DCPD) derivatives remains fast on the NMR timescale even at 103 K. Since the intramolecular exchange process could not be sufficiently slowed for spectroscopic evaluation, the conformational equilibrium is thus inaccessible by dynamic NMR. Fortunately, the spatial magnetic properties of the aryl and carbonyl groups attached to the DCPD skeleton can be employed in order to evaluate the conformational state of the system. In this context, the anisotropic effects of the functional groups in the ¹H NMR spectra prove to be the molecular response property of spatial nucleus independent chemical shifts (NICS).

Introduction

The spatial magnetic properties of molecules can be determined *via* through-space NMR shieldings (TSNMRS) and visualized as iso-chemical-shielding surfaces (ICSS).[1] This methodology[1] has been successfully applied to depict and, moreover, to quantify the anisotropic effects of functional groups and ring-current effects of aryl moieties on proton NMR chemical shifts. TSNMRS have also been employed for stereochemical assignment and to examine the diastereoisomerism of various structures.[2–14] Furthermore, anisotropic and ring-current effects, thus evaluated with respect to their influence on the proton chemical shifts, can be separated and distinguished from steric compression effects in cases where the latter contribute considerably to ¹H chemical shift differences in stereoisomers.[15,16] Finally, TSNMRS have also been employed to qualify the (anti)aromaticity[17] of push–pull compounds[18] and to evaluate quinonoid *vs.* benzenoid,[19] captodative[20] and coordinative[21] organic and inorganic compounds.

Of significant note though, there have been some recent developments of the nucleus independent chemical shifts (NICS) index[22] demonstrating that only the NICS(1)$_{zz}$ component can be rigorously used to quantify aromaticity,[23] whilst averaged NICS have proven to be generally unsuitable for the quantitative evaluation of aromaticity.[24] In addition, it should be pointed out that there are still serious reservations with regards to qualifying molecular response properties by unobservable quantities such as NICS.[24a] However, in this work we will present for the first time a definitive example of the application of spatial NICS to unequivocally assign preferred conformers even if the basic dynamic process is still too fast on the NMR timescale. This leads to the conclusion that the anisotropic effects of functional groups on the signals in ¹H NMR spectra are the molecular response property of NICS.

Our approach has also been employed to locate the precise position of ligands (inhibitors) in the binding pocket of enzymes employing the ring-current effects of the aromatic moieties of amino acid residues proximate to the ligand in the binding pocket.[4] For the same purpose, complexation induced shifts (CIS) of ligands containing aromatic rings were used by Hunter and Packer[25] and McCoy and Wyss;[26] based on this idea the latter wrote a computer program *Jsurf*.[26] This method was adopted by Hunter *et al.*,[27] incorporated into a three stage procedure and developed into a robust and flexible procedure of wide applicability, although limited to aromatic ligands.
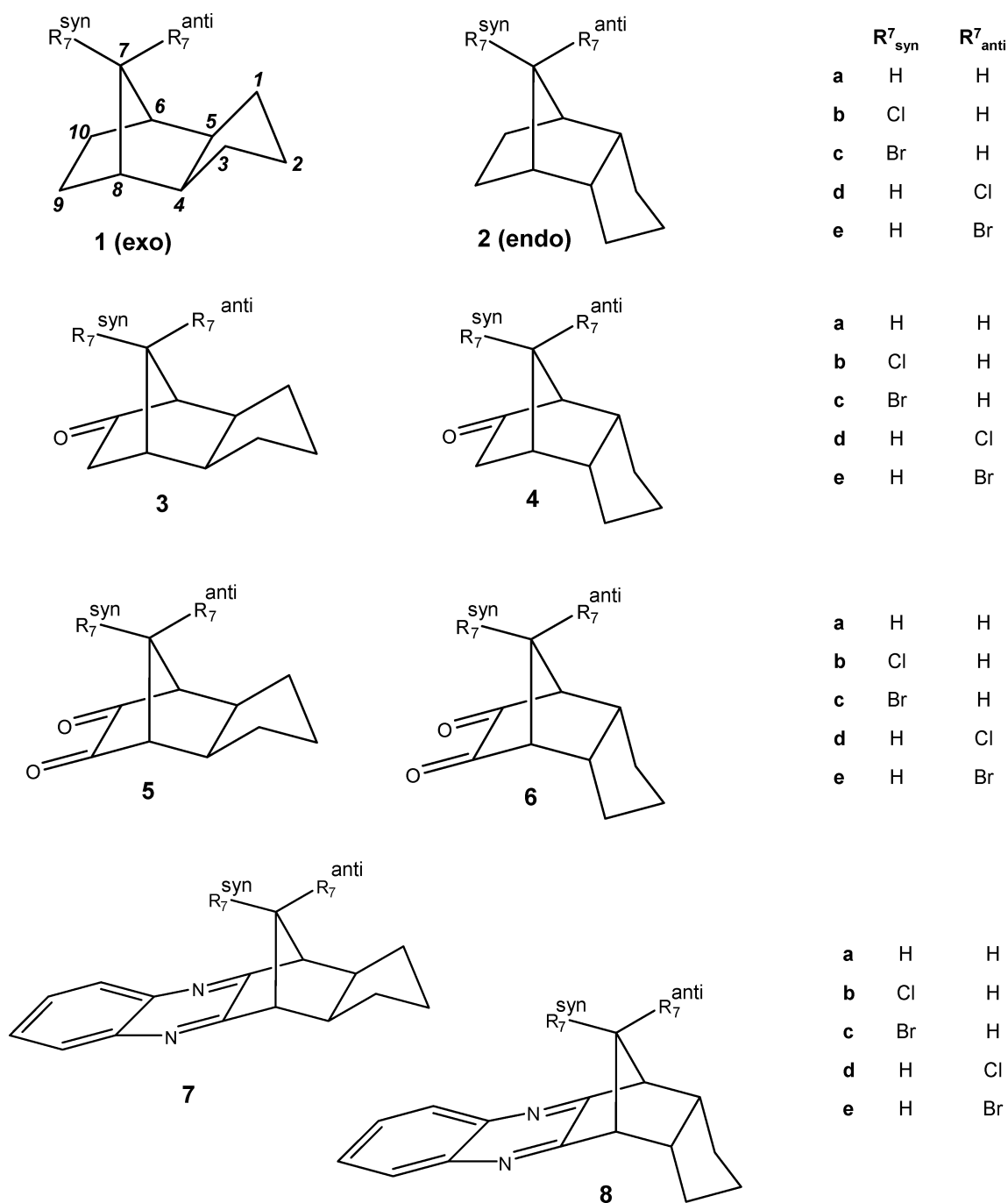
Similar approaches to estimate TSNMRS have been published by Alkorta and Elguero,[28] and Martin *et al.*[29] In both cases, shieldings of similar size and direction, comparable with the results of our approach[1] and the classical model of Bovey and Johnson[30] and Haigh and Mallion,[31,32] were obtained.

Results and discussion

Chemical syntheses and NMR spectra

Tetrahydrodicyclopentadiene (TH-DCPD) derivatives **1a**, **2a**, **4b,c**, **6b,c**, **7a** and **8a** (Scheme 1) were able to be synthesized and isolated. These compounds, along with other stereoisomers of **1–8** to complete sets of structures, were also subjected to computational examinations (*vide infra*). The parent compounds, *exo-* and

Universität Potsdam, Institut für Chemie, Karl-Liebknecht-Str. 24-25, D-14476, Potsdam (Golm), Germany. E-mail: ekleinp@uni-potsdam.de; Fax: +49-331-977-5064; Tel: +49-331-977-5210

	R^7_{syn}	R^7_{anti}
a	H	H
b	Cl	H
c	Br	H
d	H	Cl
e	H	Br

	R^7_{syn}	R^7_{anti}
a	H	H
b	Cl	H
c	Br	H
d	H	Cl
e	H	Br

	R^7_{syn}	R^7_{anti}
a	H	H
b	Cl	H
c	Br	H
d	H	Cl
e	H	Br

|	R^7_{syn}	R^7_{anti}
a	H	H
b	Cl	H
c	Br	H
d	H	Cl
e	H	Br

Scheme 1 Tetrahydrodicyclopentadiene (DCPD) derivatives **1–8**.

endo-tetrahydrodicyclopentadiene **1** and **2** were synthesized by catalytic hydrogenation of the separated DCPD isomers which provided initially the 9,10-dihydro derivatives quantitatively, prior to further hydrogenation to yield compounds **1** and **2**.[33a,b] Precursor compounds for the mono- and diketones studied were the exo/endo-1,2-DH-DCPD which were produced from exo/endo-DCPD *via* 3-step (*exo*)[34a,b] and 5-step syntheses (*endo*).[34c,d] (*endo*)Mono- (**4b**) and (*endo*)diketo derivatives (**6b**) were obtained from *exo*-DH-DCPD by reaction with *t*-butyl hypochlorite in acetic acid, saponification of the acetate and oxidation of the intermediate alcohol (*cf.* Scheme 2); the monoketone **4b**, thus obtained, was further oxidized with SeO$_2$ to the diketone **6b**. The corresponding bromo analogues **4c** and **6c** were obtained by the same procedure but using *N*-bromo succinimide instead of *t*-butyl hypochlorite.

The precursor compound **3a** for the quinoxaline derivative **7a** was synthesized by hydration of endo-DCPD with diluted sulfuric acid, hydrogenation and finally oxidation;[35] further oxidation with SeO$_2$ delivered the diketone **5a** (unstable) which quenched with *o*-phenylene diamine to **7a** (*cf.* Scheme 3).

The *exo/endo* configurations of DCPD derivatives **1–8** were assigned by [1]H[36] and ^{13}C NMR spectroscopy.[37] The detailed signal
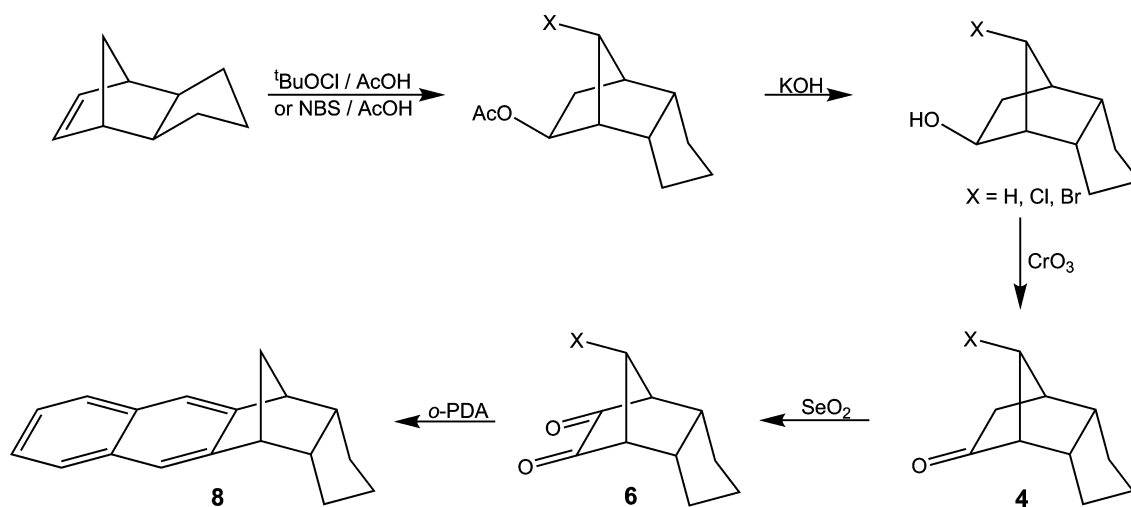
Scheme 2 Synthesis of 7-chloro(bromo)-TH-DCPD-9-ones (**4**), -diones (**6**) and the quinoxaline derivative (**8**).
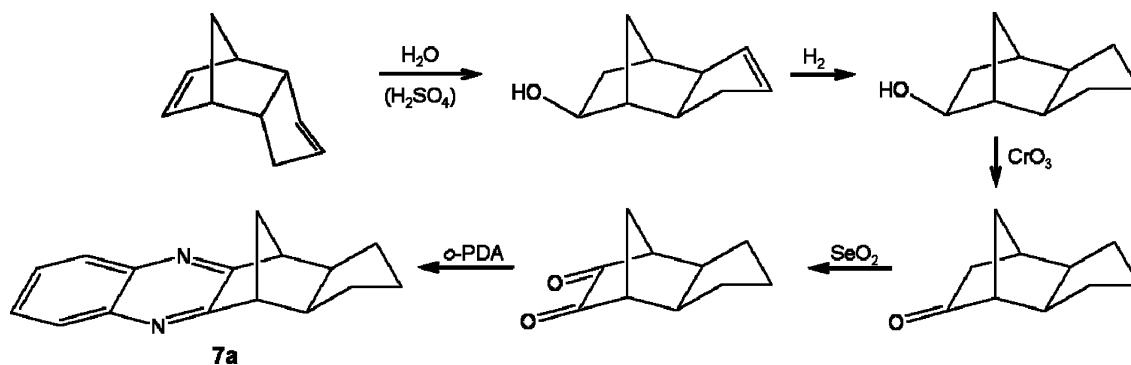

Scheme 3 Synthesis of quinoxaline derivative **7a**.

assignments of both nuclei were effected by COSY, HSQC and HMBC experiments. For the proton NMR spectra of monoketones **3** and **4**, due to severe overlap of several signals, HSQC was ineffective for assignment purposes in the relevant region but HSQC-TOCSY experiments ensured the full assignment for all ^{1}H and ^{13}C NMR signals in these cases. The experimental chemical shifts are presented in Tables 1 and 2.

Theoretical calculations

The structures of **1–8** in Scheme 1 were computed and the geometries fully optimized using the *Gaussian03*[38] program employing *ab initio* calculations at the MP2/6-311G** level.[39–41] The *exo/syn*, *exo/anti*, *endo/syn* and *endo/anti* conformers (*cf.* Scheme 4) of **1–8** were evaluated and, in order to describe the dynamic process of five-membered ring inversion, the transition states were characterized by force constants as stationary points on the potential energy surface. NMR parameters were calculated using the GIAO method[42] at the B3LYP/6-31G(d,p) level of theory by subtracting the shieldings of the protons and carbon atoms in **1–8** from tetramethylsilane (TMS) used as a reference and calculated at the same level of theory; the PCM solvent model[43] was employed to consider CDCl₃ as the solvent. Computed chemical shifts are also given in Tables 1 and 2 (*vide supra*).

Experimental ^{13}C NMR chemical shifts of TH-DCPD derivatives **1a**, **2a**, **4b,c**, **6b,c**, **7a** and **8a** (Scheme 1) measured in
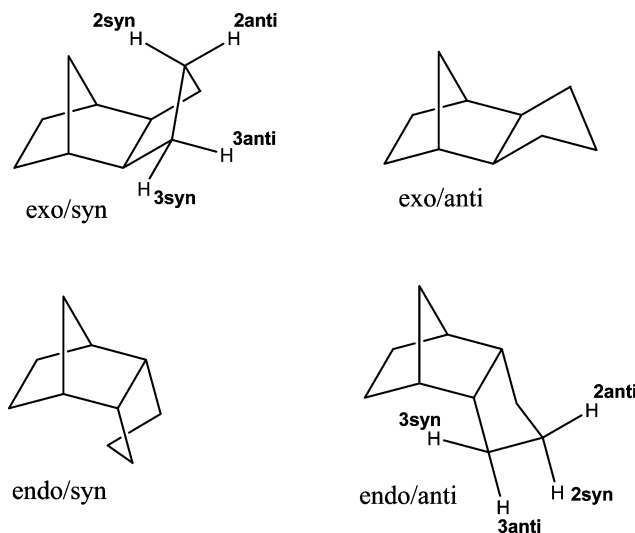
Scheme 4 Conformational equilibrium of DCPD derivatives.

CDCl₃ were correlated with the computed δ values [*cf.* Fig. 1 for $\delta(^{13}C)$]. The excellent correlation obtained was strong evidence for accurately computed structures of the compounds and, because of better correlations in the case of the *endo/syn* conformers in comparison to the *endo/anti* conformers (in the case of the *exo* isomers, only the *exo/anti* conformer was considered), the first

Table 1   ¹H Chemical shifts δ/ppm (experimental and computed at the DFT level of theory) of the DCPD derivatives **1–8**

compound	H-9 eq exp	H-9 eq calc	H-9 ax exp	H-9 ax calc	H-8 exp	H-8 calc	H-4 exp	H-4 calc	H-5 exp	H-5 calc	H-6 exp	H-6 calc	H-7 syn exp	H-7 syn calc
8a	—	—	—	—	3.43	3.26	3.11	3.05	3.11	3.05	3.43	3.26	2.17	2.01
7a	—	—	—	—	3.29	3.12	2.27	2.25	2.27	2.25	3.29	3.12	1.98	1.85
6b	—	—	—	—	3.29	2.81	3.02	2.76	3.02	2.76	3.29	2.81	Cl	Cl
6c	—	—	—	—	3.34	2.87	3.02	2.79	3.02	2.79	3.34	2.87	Br	Br
4b	2.56	2.65	2.16	2.03	2.71	2.38	2.72	2.52	2.72	2.54	2.70	2.33	Cl	Cl
4c	2.62	2.77	2.16	2.03	2.73	2.44	2.76	2.55	2.76	2.57	2.72	2.42	Br	Br
2a	1.27	1.38	1.42	1.58	2.1	2.07	2.33	2.39	2.33	2.39	2.10	2.07	1.37	1.42
1a	1.45	1.52	1.05	1.10	1.93	1.93	1.75	1.85	1.75	1.85	1.93	1.93	0.88	0.95

compound	H-7 anti exp	H-7 anti calc	H-1 anti exp	H-1 anti calc	H-1 syn exp	H-1 syn calc	H-2 anti exp	H-2 anti calc	H-2 syn exp	H-2 syn calc	H-3 anti exp	H-3 anti calc	H-3 syn exp	H-3 syn calc
8a	2.12	1.89	1.52	1.58	1.18	1.38	1.14	0.64	−0.42	−1.88	1.52	1.58	1.18	1.38
7a	2.17	2.18	2.07	2.05	1.29	1.35	1.94	1.92	1.51	1.63	2.07	2.05	1.29	1.35
6b	4.55	4.05	1.69	1.70	1.46	1.50	1.62	1.44	1.17	1.34	1.69	1.70	1.46	1.50
6c	4.38	4.16	1.69	1.71	1.48	1.51	1.64	1.44	1.18	1.36	1.69	1.71	1.48	1.51
4b	4.28	3.85	1.66	1.80	1.39	1.47	*a*	1.49	*b*	1.56	*b*	1.70	*b*	1.60
4c	4.27	4.00	*a*	1.80	1.40	1.48	*a*	1.50	*a*	1.58	*a*	1.71	*a*	1.62
2a	1.51	1.50	1.43	1.52	1.49	1.74	1.57	1.60	1.61	1.63	1.43	1.52	1.49	1.74
1a	1.31	1.50	0.92	1.06	1.82	1.87	1.59	1.61	1.13	1.27	0.92	1.06	1.82	1.87

a Range of δ, 1.75–1.50 ppm. *b* Range of δ, 1.80–1.47 ppm.

Table 2   ¹³C chemical shifts δ/ppm (experimental and computed at the DFT level of theory) of the DCPD derivatives **1–8**

compound	C-1 exp.	C-1 comp.	C-2 exp.	C-2 comp.	C-3 exp.	C-3 comp.	C-4 exp.	C-4 comp.	C-5 exp.	C-5 comp.
8a	27.88	30.29	26.78	27.45	27.88	30.29	45.91	48.79	45.91	48.79
7a	31.56	33.57	29.14	31.89	31.56	33.58	45.56	48.87	45.56	48.87
6b	28.35	30.44	27.03	28.97	28.35	30.44	43.57	46.52	43.57	46.51
6c	28.41	30.60	27.06	28.92	28.41	30.60	44.50	47.26	44.50	47.26
4b	28.26	30.04	27.37	29.51	27.63	30.48	41.33	43.75	43.06	46.24
4c	28.38	30.10	27.66	29.39	27.66	30.65	41.51	44.14	43.90	46.94
2a	26.95	29.94	28.77	30.51	26.95	29.94	45.53	47.27	45.53	47.27
1a	32.43	34.31	27.24	29.48	32.43	34.31	48.22	50.16	48.22	50.16

compound	C-6 exp.	C-6 comp.	C-7 exp.	C-7 comp.	C-8 exp.	C-8 comp.	C-9 exp.	C-9 comp.	C-10 exp.	C-10 comp.
8a	48.60	49.97	48.12	47.74	48.60	49.97	162.68	158.02	162.68	158.02
7a	48.28	49.40	38.54	40.65	48.28	49.41	164.85	160.33	164.85	160.33
6b	61.12	62.07	57.11	61.51	61.12	62.07	199.66	197.77	199.66	197.77
6c	60.99	62.54	45.42	58.46	60.99	62.54	199.33	197.21	199.33	197.21
4b	62.26	62.89	64.21	67.29	45.33	47.59	36.58	37.78	213.80	205.13
4c	62.79	63.89	54.65	65.28	45.45	48.20	37.50	38.29	213.72	205.11
2a	41.57	44.32	43.30	43.27	41.57	44.32	23.06	26.16	23.06	26.16
1a	40.68	42.47	32.08	33.42	40.68	42.47	28.77	31.48	28.77	31.48

hint for these *endo/syn* structures as the preferred, or at least higher populated conformers, was obtained. The corresponding correlations of proton chemical shifts are not given because of significant signal overlap in the experimental ¹H NMR spectra.

To calculate the NICS,[44] ghost atoms were placed within a lattice of −10 Å to +10 Å utilizing a step size of 0.5 Å in all three directions of the Cartesian coordinate system. The zero points of the coordinate system were positioned at the centers of the quinoxalyl moiety in **7** and **8** and at the centers of the carbonyl groups in **3–6**. The resulting 68,921 NICS values obtained

were analyzed and visualized by SYBYL 7.3 molecular modeling software;[45] different ICSS of −0.1 ppm (red) deshielding and 5 ppm (blue), 2 ppm (cyan), 1 ppm (green-blue), 0.5 ppm (green) and 0.1 ppm (yellow) shielding, were used to visualize the TSNMRS of **1–8** (*cf.* Fig. 5, *vide infra*).

Dynamic NMR spectroscopy

The ¹H NMR spectra were first recorded at room temperature. The five-membered ring attached to the rigid TH-DCPD skeleton

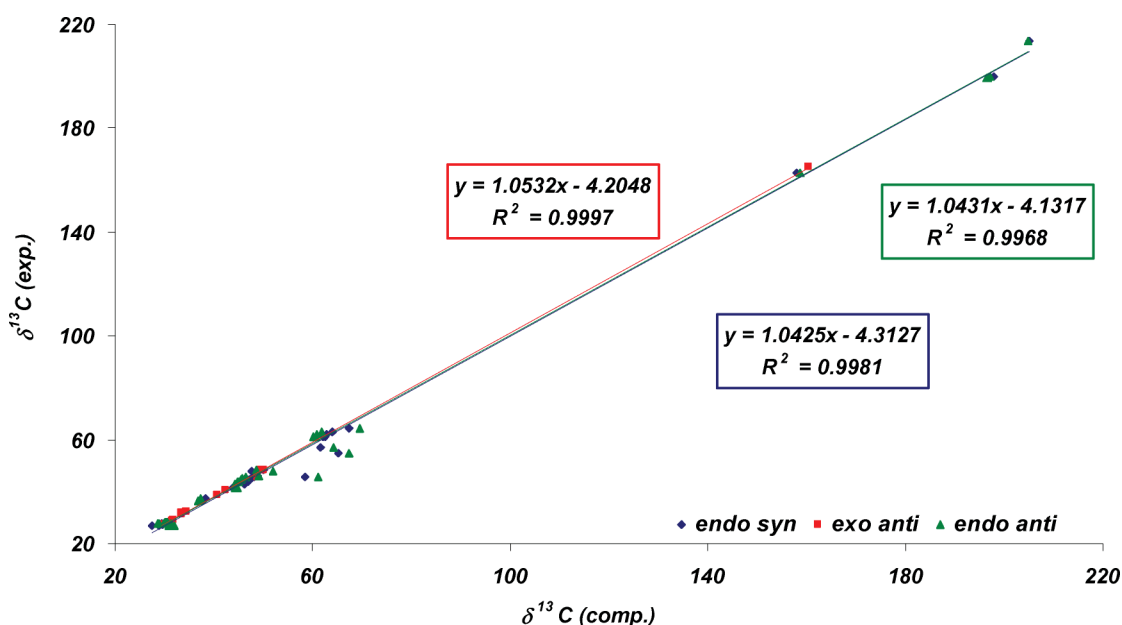$$y = 1.0532x - 4.2048$$
$$R^2 = 0.9997$$

$$y = 1.0431x - 4.1317$$
$$R^2 = 0.9968$$

$$y = 1.0425x - 4.3127$$
$$R^2 = 0.9981$$

◆ *endo syn*   ■ *exo anti*   ▲ *endo anti*

Fig. 1   Correlation of computed $\delta(^{13}C)$ *vs.* experimental $\delta(^{13}C)$ for DCPD derivatives **1a**, **2a**, **4b,c**, **6b,c**, **7a** and **8a** (*cf.* Scheme 1).

should be highly flexible and, moreover, rapidly interconverting on the NMR timescale at this temperature. To the best of our knowledge, this dynamic ring inversion process has not been studied previously (Scheme 4). Because extremely low barriers to ring inversion were expected,[46] the compounds were dissolved in a freon mixture (CD$_2$Cl$_2$/CHFCl$_2$/CHF$_2$Cl = 1 : 1 : 3) and variable-temperature ^{1}H NMR spectra recorded in steps down to 103 K (*cf.*

Fig. 2 for compound **8a**). The proton signals did broaden upon lowering of the temperature, with the strongest effects observed for the protons of the five-membered ring. However, none of the signals were observed to decoalesce into distinct conformer signals. The same result was also obtained for the remaining *endo* and the corresponding *exo* isomers studied, whereby decoalescence of the signals was not observed.
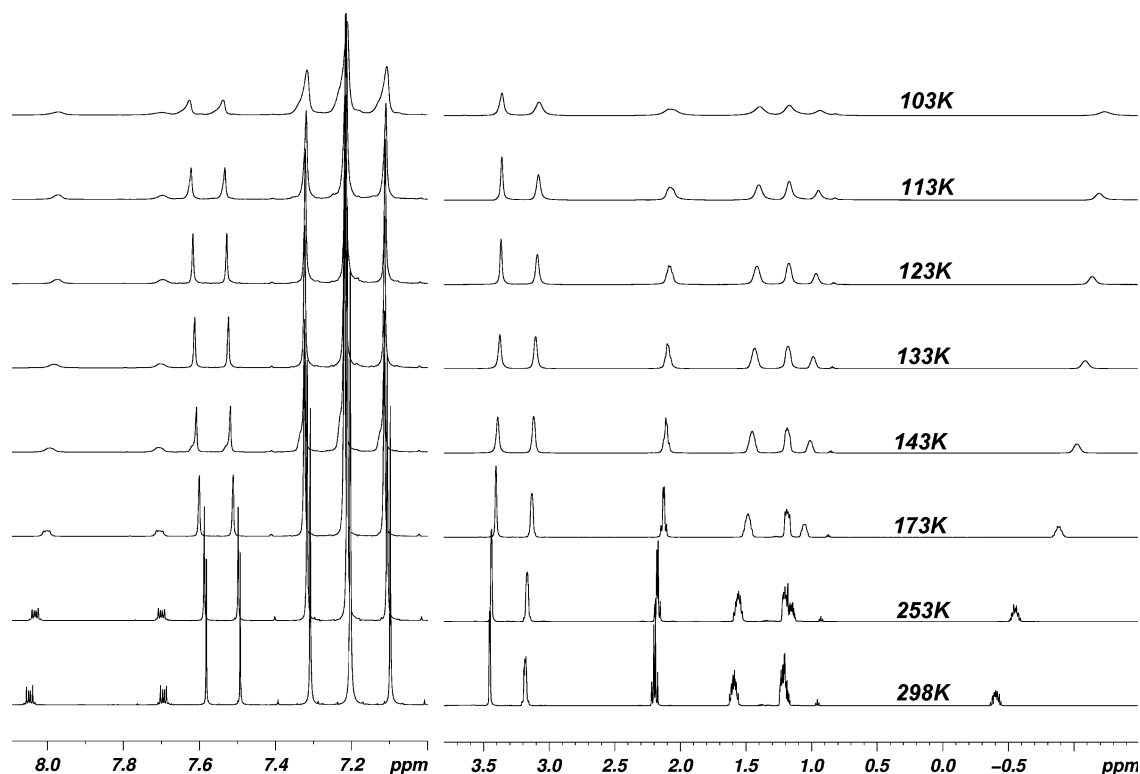

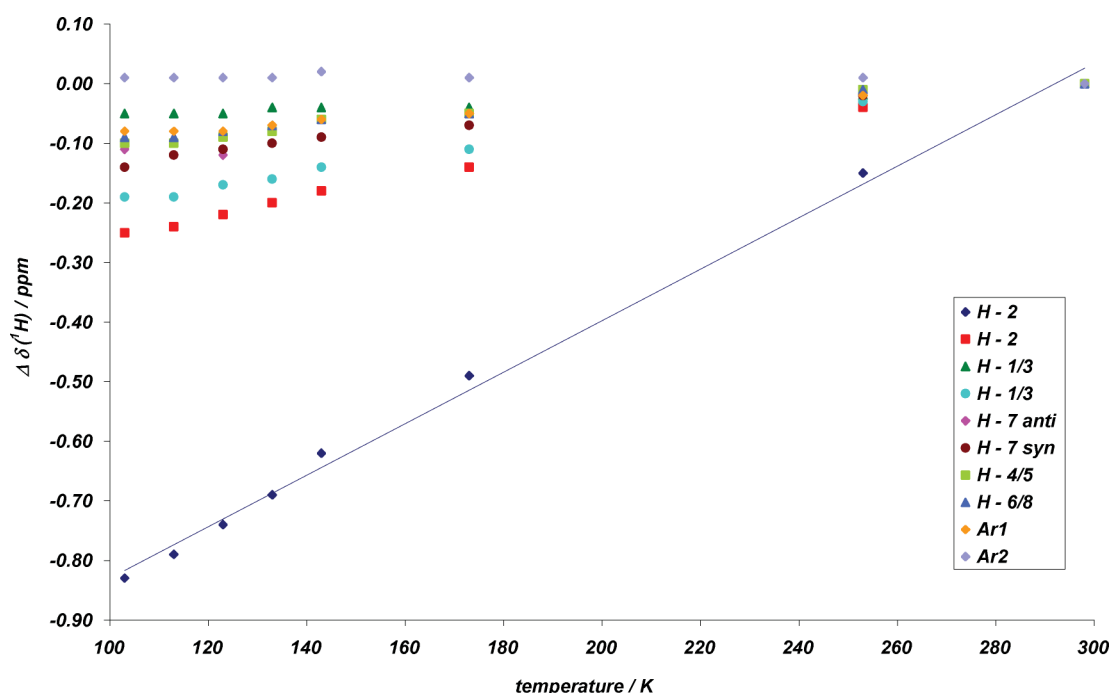**Fig. 2**   Variable temperature ^{1}H NMR spectra of compound **8a**.

Fig. 3 Variable temperature ¹H chemical shifts of the protons of **8a**.

For the *endo* isomers, the proton signals were observed to shift upon reduction of the temperature (*cf.* Fig. 3). The shielding shift of the two C-2 protons was extraordinary, with chemical shift differences of *ca.* −0.3 and −0.9 ppm, respectively, observed upon going from 298 to 103 K. Feasible interpretations of these observations include that (i) the five-membered ring inversion remains fast on the NMR timescale (even at 103 K), and that (ii) due to $K = [syn]/[anti]$, $-\Delta G° = RT \ln K$, the conformational equilibrium is increasingly shifted to one side (in all probability to the *endo/syn* conformer because of the extremely high field position of the H-2 signals as a result of the ring-current effect of the aromatic moiety in **8a**, *vide infra*). The change in position of the proton signals in the *exo* isomer **7a** upon a reduction in temperature is much smaller, < 0.05 ppm usually, however, it is to lower field in complete contrast to the *endo* isomer protons. Because the *exo* isomers are elongated molecules with the *exo/anti* preferred conformer (*vide infra*), these small deshielding observations are consistent with expectations: in the *exo* DCPD derivative **7**, all protons on the DCPD skeleton lie in-plane with the quinoxalyl moiety and can thus experience deshielding due to the

ring-current effect (*cf.* Fig. 5, *vide infra*). Structural differences, due to *syn/anti* conformers, are far away from the aromatic moiety. Thus, in agreement with the experiment, only negligible low temperature chemical shift gradients could be expected and from the low temperature shifts of the *exo* diastereomers, conclusions similar to the conformational equilibrium of the *endo* diastereomers cannot be drawn.

Computation of the proton chemical shift differences of the C-2 protons in **8a** (*syn/anti* conformers) yielded $\Delta\nu$ in excess of 1900 and 500 Hz. With the lowest temperature obtained with our equipment 103 K for T_c, both rate constants k_c of 4221 and 1111, respectively, and a barrier to ring inversion below 4.1–4.4 kcal mol⁻¹ for $\Delta G^{\neq}$, can be suggested. Hence, the experimentally observed extreme broadening of the C-2 protons at 103 K corroborates the anticipated low barrier to ring inversion.

The dynamic process was also examined by the theoretical treatment yielding two interesting results (*cf.* Table 3): For the *endo* configurations **2a**, **4a**, **6a** and **8a**, the *syn* conformers are at least 1.61 kcal mol⁻¹ more stable than their corresponding *anti* analogues (in the *exo* isomers **1a**, **3a**, **5a** and **7a**, the *anti* conformers

Table 3 Computation of the five-membered ring inversion of DCPD derivatives **1a**–**8a**; energies E [kcal mol⁻¹]

Compound	Ground states *exo/anti* or *endo/syn*	(preferred conformers) *exo/syn* or *endo/anti*	Transition state	Barrier to five-membered ring inversion
1a	0.00	2.14	4.59	4.59 (2.45)
2a	0.00	1.61	5.21	5.21 (3.60)
3a	0.00	2.08	4.66	4.66 (2.58)
4a	0.00	1.62	5.02	5.02 (3.40)
5a	0.00	2.06	4.81	4.81 (2.75)
6a	0.00	1.98	5.48	5.48 (3.50)
7a	0.00	1.98	4.53	4.53 (2.56)
8a	0.00	2.29	5.29	5.29 (3.00)

are, as expected, more stable by at least 1.98 kcal mol^{-1}, *cf.* Table 3) and the barrier to ring inversion is low as expected (2.45–5.48 kcal mol^{-1}) from experimental examination of $\Delta G^{\neq}$.

To summarize the results thus far, the five-membered ring inversion dynamic process remains fast on the NMR timescale even at 103 K—though very near to coalescence—and the *syn* conformers in the *endo* isomers are, surprisingly, the preferred conformers. Low-temperature shifts of the protons in the *exo/endo* diastereomers were observed which are different in both directions (shielding in *endo* and deshielding in *exo*, respectively) and size (strongest low-temperature shifts for H-2 protons in *endo*) which, due to $K = [syn]/[anti]$ and $-\Delta G^{\circ} = RT \ln K$, point to further increasing population of the *endo/syn* conformer. Similar conclusions concerning the *syn/anti* conformational equilibrium of the *exo* diastereomers, due to only negligible low temperature chemical shift gradients, cannot be drawn. Thus, full experimental proof for the preferred conformers of the *exo/endo* isomers has not been obtained.

Spatial magnetic properties of quinoxalyl and carbonyl moieties for the preferred DCPD conformers

For the aforementioned reason, the spatial magnetic properties (*i.e.* TSNMRS) of the carbonyl groups in **3–6** and of the quinoxalyl moiety in **7** and **8** were calculated and ^{1}H chemical shift differences, $\Delta\delta$, in the ^{1}H NMR spectra relative to the reference compounds **1** and **2** evaluated (*cf.* Table 1). The procedure and conclusions are described for the quinoxalyl derivatives **7a** and **8a** and can be taken as examples for the other cases.

In Fig. 4, the experimental ^{1}H NMR spectra of the *exo* and *endo* isomers, **7a** and **8a**, respectively, at room temperature

are presented. Three protons in each isomer are highlighted to emphasize characteristic differences: Whilst H-4,5(*endo*) in **8a** are deshielded compared with H-4,5(*exo*) in **7a**, one of the H-1,3 protons and one H-2 proton are strongly shielded whilst the others are only moderately shielded in the comparison of *exo* **7a** and *endo* **8a**. In Fig. 5, the calculated structures of the four conformers of **7a** and **8a**, *exo/syn*, *exo/anti*, *endo/anti* and *endo/syn*, are presented. For the various conformers, the TSNMRS of the quinoxalyl moity are visualized as ICSS of various magnitude and sign [−0.1 ppm (red) deshielding and 5 ppm (blue), 2 ppm (cyan), 1 ppm (green-blue), 0.5 ppm (green) and 0.1 ppm (yellow) shielding]. Careful examination of the depictions in Fig. 5 corroborates well the conclusions of the previous sections with the following points noted.

(i) Firstly, the protons H-4,5, which are *endo* in **7** and *exo* in **8** and which are not very dependent on the five-membered ring inversion, can be employed as comparative references. In the *exo* isomer, H-4,5 are positioned below the 0.1 ppm shielding ICSS and proximate to the 0.5 ppm ICSS [precisely, $\Delta\delta = 0.16$ ppm (*syn*) and 0.21 ppm (*anti*)] whilst in the *endo* isomer, the same protons are found inside the red (−0.1 ppm) deshielding ICSS (precisely, $\Delta\delta = -0.34$ ppm). The sufficiently good agreement of $\Delta\delta = 0.50$ ppm and 0.55 ppm, respectively, and the correct sign (shielded in **7a** and deshielded in **8a**) with respect to the experimental observation ($\Delta\delta = 0.91$ ppm) is most promising. It should be not forgotten that the anisotropic effect of the aryl moiety is only one effect influencing the ^{1}H chemical shift as there is also steric compression which propels the proton chemical shift in the opposite direction[15,16] and which, furthermore, is quite capable of masking the anisotropic effect altogether.[8] With regards to the other protons of the five-membered ring, the ring-current effect of
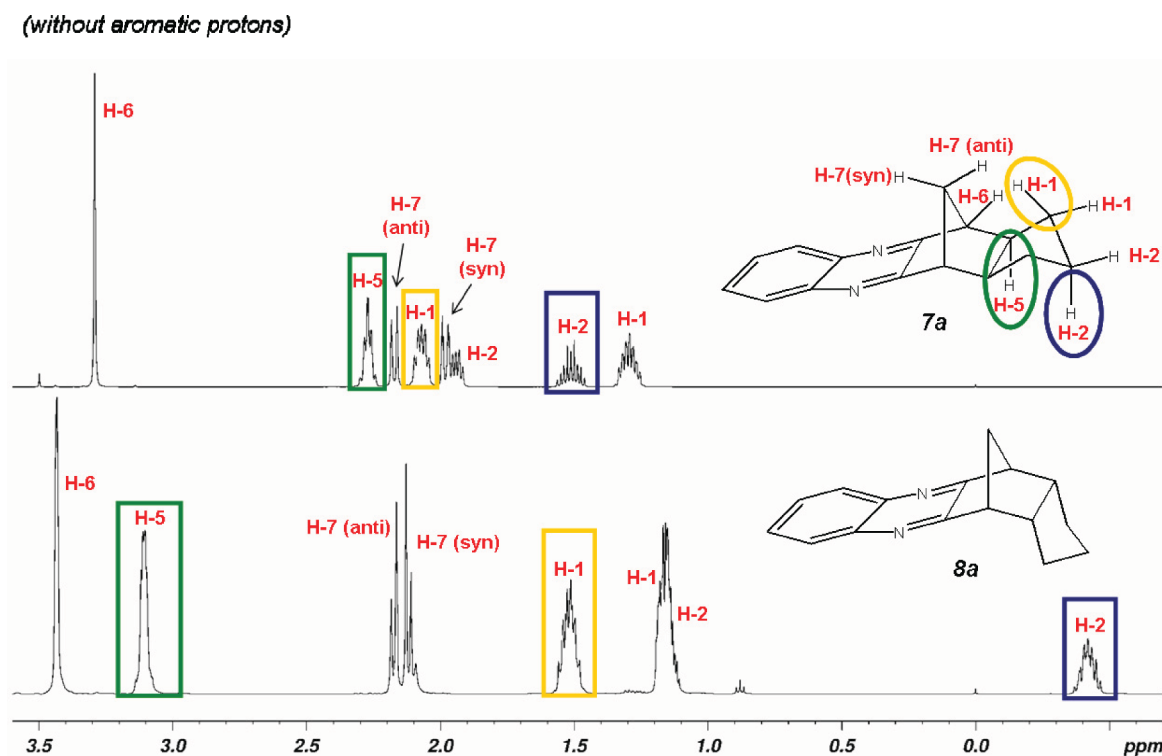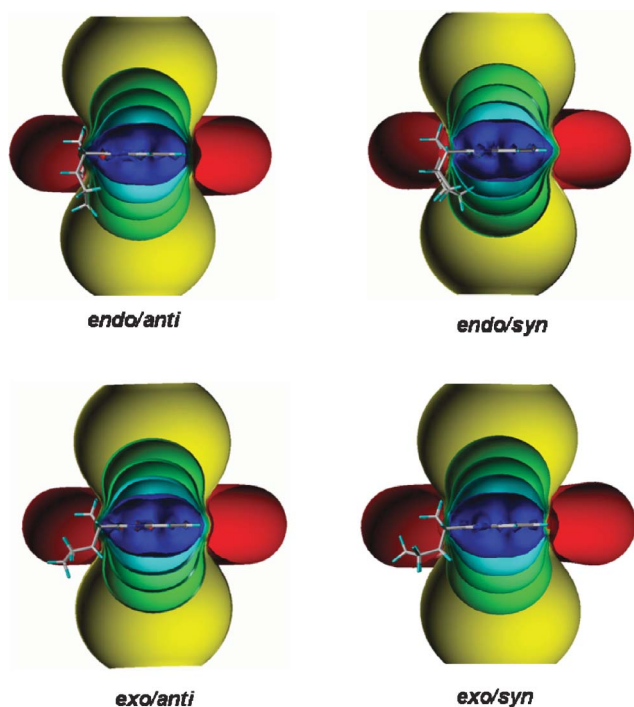

(without aromatic protons)

Fig. 4 ^{1}H NMR spectra of *exo* **7a** and *endo* isomers **8a**.

Fig. 5 Structures of *syn/anti* conformers of *exo/endo* isomers **7a** and **8a** together with the ring-current effect of the quinoxalyl moiety visualized as ICSS of various size and direction [−0.1 ppm (red) deshielding and 5 ppm (blue), 2 ppm (cyan), 1 ppm (green-blue), 0.5 ppm (green) and 0.1 ppm (yellow) shielding].

the quinoxalyl moiety is decisively dependent on both the *exo/endo* configuration and the *syn/anti* conformation of the attached five-membered ring.

(ii) For the *exo* configuration, both the H-1,3 and H-2 protons are well away from any shielding influences. Actually, in the two *syn/anti* conformations they are positioned inside the −0.1 ppm deshielding ICSS (precisely, $\Delta\delta = -0.28$ ppm or up to −0.01 ppm only), or even outside of it with even smaller influence of the ring-current effect of the aryl moiety on the corresponding proton chemical shifts. Hence, the ring-current effect of the attached aryl moiety does not provide any influential effects concerning the preferred conformer of the *exo* isomer and it remains that the *exo/anti* conformer has the higher computed stability compared to its *exo/syn* analogue (*vide supra*).

(iii) A different situation exists for the *endo* isomers. In the *anti* conformation, the H-1,3(*syn*) protons are positioned below the 1 ppm shielding ICSS whilst the corresponding H-1,3(*anti*) protons are outside the 0.1 ppm ICSS (precisely, $\Delta\delta = 0.92$ ppm and 0.08 ppm, respectively). The same H-1,3 protons in the corresponding *syn* conformation are found below the 0.1 ppm shielding ICSS (precisely, $\Delta\delta = 0.24$ ppm and 0.13 ppm, respectively). Compared with the experimental chemical shift differences ($\Delta\delta = 0.48$ ppm and 0.07 ppm, respectively), the direction of the chemical shift changes is correct (the two H-1,3 signals are shielded in the *endo* isomers compared with the *exo* isomers), but the magnitude of the shifts indicates a preference for the *endo/syn* conformer. As already mentioned, the second effect on the ¹H chemical shift is steric compression and increased steric hindrance deshields the corresponding proton so that the computed shieldings of one H-1,3 proton by more than 1 ppm compared with the experimental

Table 4 Experimental ¹H chemical shift differences opposed to the ring-current effect of the aryl moiety in **7a** and **8a**

Proton	$\Delta\delta_{exp}$[a]	*exo/anti*[b]	*exo/syn*[b]	*endo/anti*[b]	$\Delta\Delta\delta$[c]	*endo/syn*[b]	$\Delta\Delta\delta$[d]
H-4,5	**0.84**	0.16	0.21	−0.34	0.50	−0.34	**0.50**
					0.55		**0.55**
H-1,3	**−0.55**	−0.28	−0.26	0.92	1.20	**0.24**	**0.52**
					1.18		**0.50**
	−0.11	−0.14	−0.08	0.08	0.22	**0.13**	**0.27**
					0.16		**0.21**
H-2	**−0.80**	−0.1	−0.01	0.14	0.24	**0.50**	**0.60**
					0.15		**0.51**
	−1.93	−0.25	−0.12	0.72	0.97	**2.62**	**2.87**
					0.84		**2.74**

[a] Experimental chemical shift differences of the corresponding protons between **7a** and **8a**. [b] Ring-current effect (*cf.* Fig. 5) of the quinoxalyl moiety in the four conformers (*cf.* Scheme 4) of **7a** and **8a**. [c] Chemical shift differences of the ring-current effect of the quinoxalyl moiety between the conformers *endo/anti* and *exo/anti* and *exo/syn*, respectively. [d] Chemical shift differences of the ring-current effect of the quinoxalyl moiety between the conformers *endo/syn* and *exo/anti* and *exo/syn*, respectively.

value of only 0.48 ppm could be conceivable, but together with point (iv) this is less probable.

(iv) Protons H-2 in the *endo* isomers are the most strongly influenced by the ring-current effect of the aryl moiety and readily clarify the conformational state. In the *syn* conformation, the H-2(*syn*) proton is positioned below the 2 ppm ICSS (precisely, $\Delta\delta = 2.62$ ppm) and the corresponding H-2(*anti*) proton exactly at the 0.5 ppm ICSS (precisely, $\Delta\delta = 0.50$ ppm). Less notable effects are observed in the corresponding *anti* conformer where the H-2(*syn*) proton is positioned between the 0.5 ppm shielding ICSS and the 1 ppm shielding ICSS (precisely, $\Delta\delta = 0.715$ ppm) and H-2(*anti*) is below the 0.1 ppm shielding ICSS (precisely, $\Delta\delta = 0.14$ ppm). Compared with the experimental chemical shift differences ($\Delta\delta = 0.76$ ppm and 1.98 ppm, respectively), the direction of the proton chemical shifts changes are in agreement (the *endo* isomer compared with the *exo* isomer is shielded) and similarly for the $\Delta\delta$ values as well. The ring-current effect on H-2(*syn*), due to extreme steric compression, is overestimated ($\Delta\delta = 2.87$ ppm) and the difference to the experimental value of $\Delta\delta = 1.91$ ppm originates from steric hindrance for this proton.[15,16]

All experimental and computed ¹H chemical shift differences are given in Table 4; $\Delta\delta_{exp}$ and $\Delta\delta_{calc.}$ for the *endo*(*syn*) conformer compared with the *endo*(*anti*) conformer are highlighted and strikingly corroborate this structure as the preferred conformer of the DCPD derivative **8a**.

As another proof for the preferred *exo/anti* conformer of **7a** and the *endo/syn* conformer of **8a**, the H,H-coupling constants of these conformers and also of the corresponding *exo/syn* and *endo/anti* conformers (the comparison of experimental and calculated coupling constants were successfully employed in conformational analysis),[47] were computed at the same level of theory: the values are given in Table 5 together with the experimental coupling constants which were obtained by PERCH simulation[48] of the ¹H NMR spectra of **7a** and **8a**, respectively. The agreement between simulated and experimental spectra (*cf.* Fig. 6 and 7) prove to be excellent, hence, realistic coupling constants were obtained in contrast to present signal overlap, many long range H,H coupling constants and second order effects. If the experimental coupling constants are compared with the theoretical values as calculated

Table 5 Experimental H,H-coupling constants of both *exo* isomer **7a** and the *endo* isomer **8a**, together with the corresponding values as calculated for the corresponding conformers *exo/syn*, *exo/anti*, *endo/syn* and *endo/anti*, respectively

| Proton | $^3J_{H,H}$ coupling constants (Hz) | | |
| | Exp. | Calc. | |
		exo/syn	*exo/anti*
6,5	0.43	0.64	0.63
6,4	−0.71	−0.70	−0.65
6,8	0.07	0.73	0.51
6,7syn	1.49	1.27	1.42
6,7anti	1.45	1.51	1.35
6,1anti	−0.16	−0.33	−0.13
6,1syn	0.19	0.13	−0.03
5,4	8.76	6.78	8.13
5,7syn	1.51	0.89	0.83
5,1anti	8.33	9.40	7.64
5,7anti	−0.37	−0.51	−0.50
5,2anti	−0.29	−0.04	−0.06
5,1syn	8.82	0.68	8.00
5,2syn	−0.73	−0.78	−0.84
7syn, 7anti	−10.52	−9.20	−9.15
1anti, 4	−0.15	−0.19	−0.16
1anti, 3anti	1.90	−0.15	1.14
1anti, 2anti	6.70	8.02	5.67
1anti, 1syn	−12.53	−12.30	−11.20
1anti, 2syn	1.22	10.90	0.42
2anti, 1syn	12.75	0.35	11.40
2anti, 2syn	−12.27	−11.80	−10.70
1syn, 4	−0.53	−0.87	−0.64
1syn, 3anti	−0.34	−0.81	−0.56
1syn, 3syn	0.37	0.59	0.07
1syn, 2syn	6.52	7.41	5.39
6,5	4.88	4.78	4.52
6,4	0.26	−0.10	−0.07
6,8	1.61	0.73	0.52
6,7syn	1.38	1.48	1.56
6,7anti	1.65	1.27	1.22
6,1syn	0.08	−0.10	−0.27
6,1anti	−0.15	−0.49	−0.11
5,4	10.06	8.35	10.52
5,7syn	−0.03	−0.40	−0.40
5,1syn	3.50	0.56	8.28
5,7anti	0.38	0.23	0.24
5,2syn	−0.33	−0.84	−0.80
5,1anti	9.38	8.71	7.63
5,2anti	0.30	0.07	−0.04
7syn, 7anti	−9.63	−8.28	−8.33
1syn, 4	−0.59	−0.77	−0.61
1syn, 3syn	0.71	0.58	0.12
1syn, 2syn	7.30	7.31	5.51
1syn, 1anti	−13.52	−11.94	−11.62
1syn, 2anti	4.22	0.38	11.52
2syn, 1anti	9.32	10.71	0.43
2syn, 2anti	−13.06	−12.39	−10.73
1anti, 4	−0.29	−0.25	−0.31
1anti, 3syn	−0.46	−0.75	−0.57
1anti, 3anti	0.18	−0.12	0.79
1anti, 2anti	7.74	7.74	5.79

for the various conformers, the agreement between experiment and *exo/anti* and disagreement with *exo/syn* completely confirms in case of **7a** our aforementioned results—*exo/anti* proves to be the anancomeric stereoisomer of **7a**. This is clearly corroborated if the two theoretical spectra, on basis of computed H,H coupling constants, are compared with the experimental ¹H NMR spectrum of this compound (*cf.* Fig. 8); only in the case of *exo/anti* is there agreement, actually already complete agreement,

Table 6 Anisotropic effects (as TSNMRS) of carbonyl group(s) on five-membered ring protons in **3–6**

Compound	Protons	Δδ(*exo/anti*)	Δδ(*exo/syn*)	Δδ(*endo/anti*)	Δδ(*endo/syn*)
3/4	H-4/5	−0.015 (0.28)	—	−0.13 (−0.03)	**−0.125**
5/6	H-4/5	0.21	—	−0.16	**−0.17**
3/4	H-1/3	−0.01 (−0.04)	—	0.12 (0.515)	**0.1 (0.275)**
5/6	H-1/3	−0.04 (−0.13)	—	0.1 (0.54)	**0.1 (0.29)**
3/4	H-2	−0.02 (0.0)	—	0.1 (0.04)	**0.14 (0.42)**
5/6	H-2	−0.04 (−0.02)	—	0.18 (0.065)	**0.26 (0.78)**

which, on the other hand, confirms that now-a-days computational possibilities provide coupling constants with "analytical precision".

The same conformational analysis of the *endo* isomer **8a** is less clear. For sure, there is better agreement between experiment and calculation in case of *endo/syn*, however, for ³J[5,1(*syn*)] and ³J[1(*syn*),2(*anti*)] major differences were observed (*endo/syn*: calculated 0.56 Hz and 0.38 Hz, respectively, but experimental values are 3.50 Hz and 4.22 Hz, respectively) which point to an existing conformational equilibrium with two adequately populated conformers. Boltzmann weighting [employing as boarder case in addition to the values of *endo/syn* (*vide supra*) the corresponding *endo/anti* coupling constants which are 8.28 Hz and 11.52 Hz, respectively] delivered coincident results: 62% to 66% *endo/syn* and 34% to 38% *endo/anti*. With this result in hand, it is clear why simulated ¹H NMR spectra on basis of calculated coupling constants of both conformers *endo/syn* and *endo/anti*, respectively, did not agree with the experimental proton NMR spectrum of **8a** and why the protons in **8a** are high field shifted when lowering the temperature. The population of *endo/syn*, the more stable conformer, increases with lowering the temperature on behalf of *endo/anti* in complete agreement with the conclusions drawn from the spatial magnetic properties of these structures.

Anisotropic effect of carbonyl group(s) on the ¹H NMR spectra of DCPD derivatives

The same methodology can now be applied to study the anisotropic effect of one (for **3** and **4**) and two carbonyl groups (for **5** and **6**) on the ¹H NMR spectra of these compounds relative to compounds **1** and **2**. As for the aryl moiety in **7** and **8**, the ring protons H-1 to H-5, which are dependent on the *exo/endo* configuration and the *syn/anti* conformation, can be duly considered (the corresponding Δδ TSNMRS data of the anisotropic effects on the corresponding ¹H chemical shifts are given in Table 6).

In the *exo* isomers (for both *syn* and *anti* conformations), these protons are too distant from the carbonyl moieties and do not experience anisotropic effects and thus were not, except for H-4,5, considered. Although anisotropic effects on the latter protons are small (maximum 0.21 ppm), the direction of the shift is, however, reversed in the *exo/endo* isomers, where remarkable chemical shift differences of up to Δδ = 0.4 ppm could be generated.

The anisotropic effects of the carbonyl groups on the proton chemical shifts are more intense in the *endo* isomers for both *syn* and *anti* conformations. The protons *syn* to the carbonyls of the H-1,3 methylene groups in the *anti* conformation and the proton *syn* to the carbonyls of the H-2 methylene group are strongly
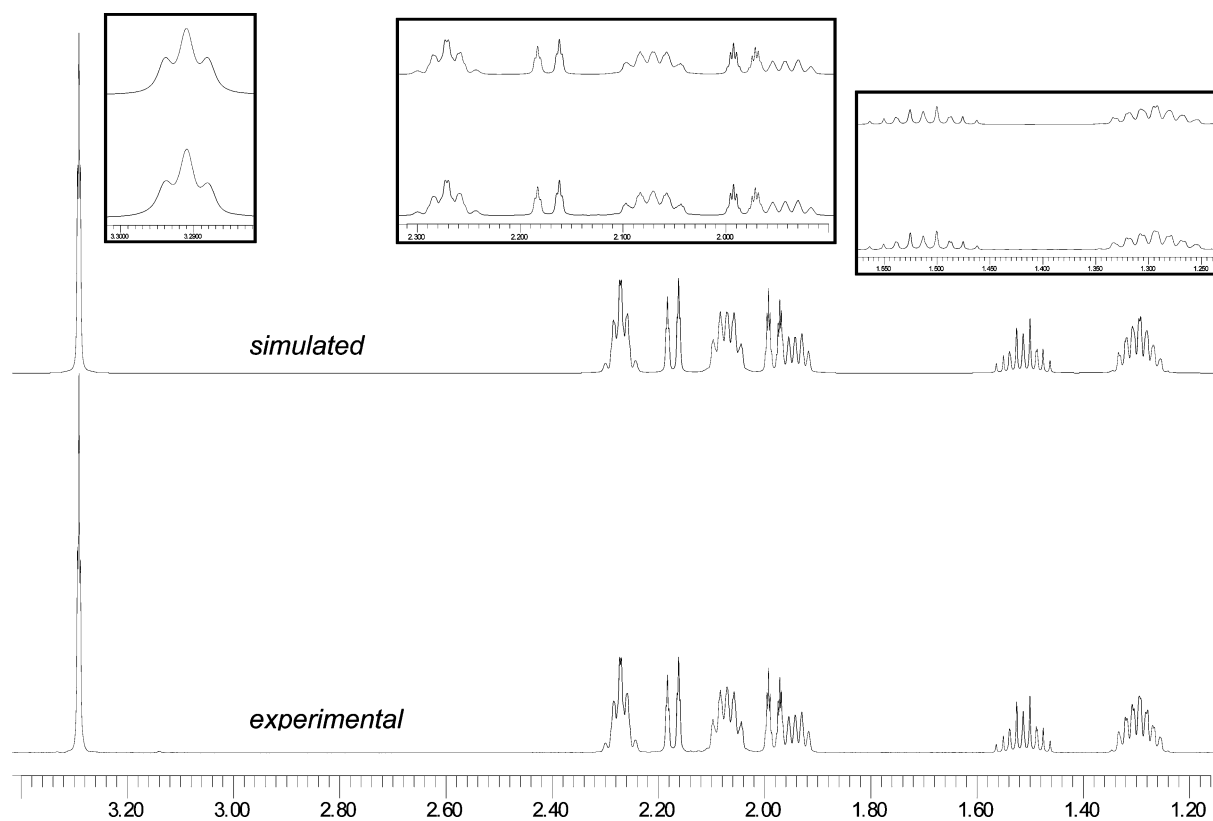
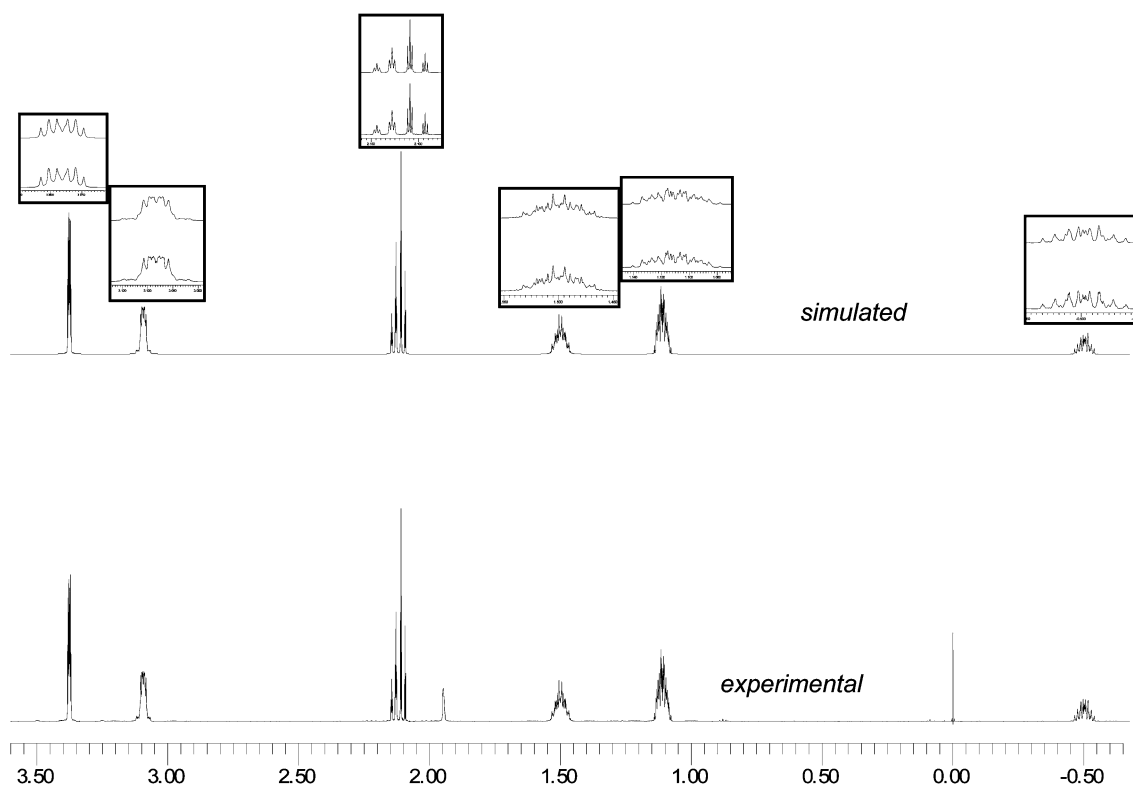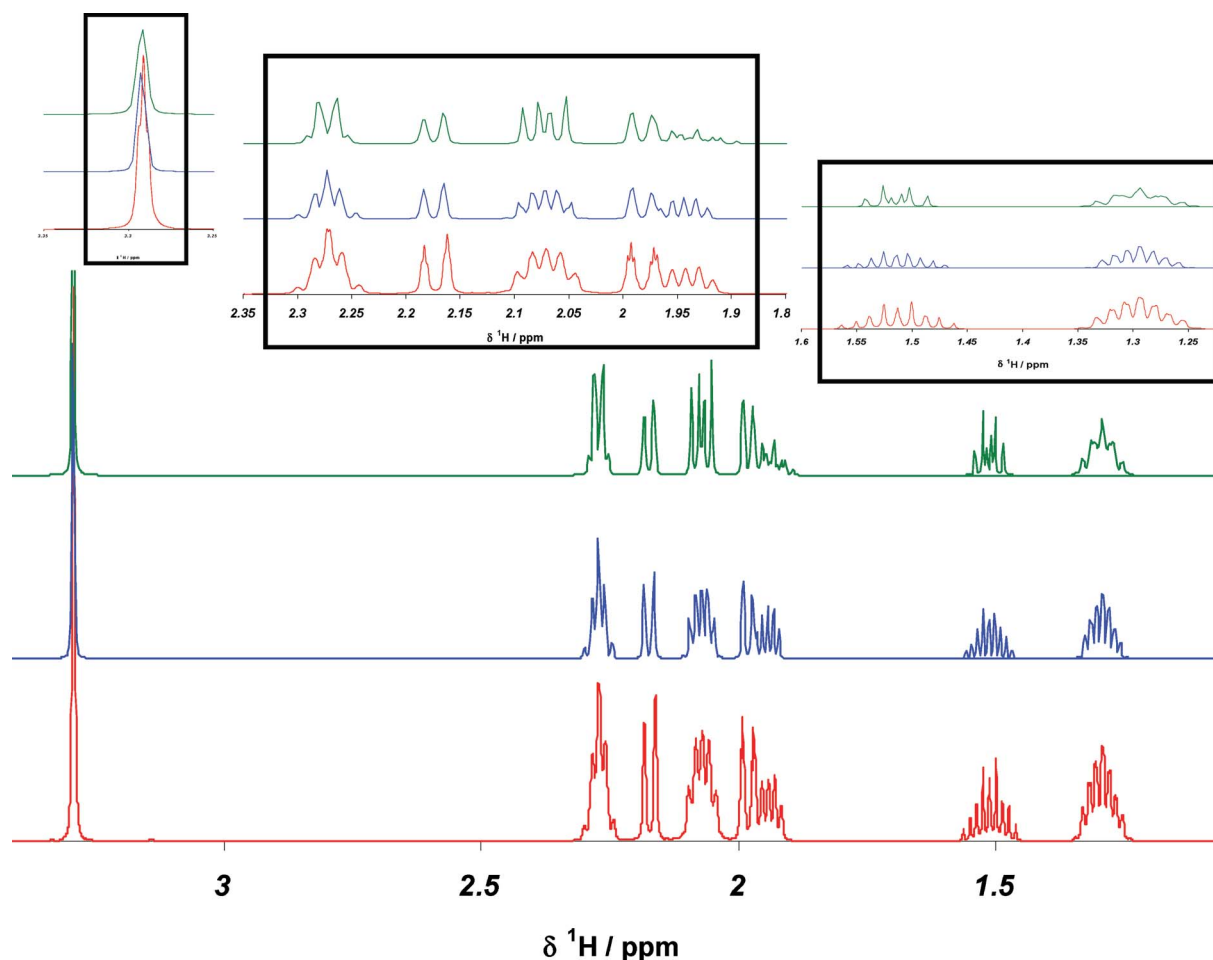**Fig. 6** Experimental and PERCH-simulated[48] ^{1}H NMR spectrum of the *exo* diastereomer **7a**.

Fig. 7 Experimental and PERCH-simulated[48] ^{1}H NMR spectrum of the *endo* diastereomer **8a**.

Fig. 8 Computed ¹H NMR spectra of *exo/syn* (green) and *exo/anti* conformers (blue) of **7a** in comparison with the corresponding experimental (red) proton NMR spectrum of this compound.

shielded ($\Delta\delta = 0.54$ ppm and up to 0.78 ppm, respectively), the corresponding protons *anti* to the carbonyls are shielded as well but only to a minor degree ($\Delta\delta = 0.1$ ppm and up to 0.29 ppm, respectively). The same is also true for the *syn* H-2 proton. In the case of the monocarbonyl compound, $\Delta\delta = 0.42$ and 0.78 ppm in comparison to the corresponding *endo* dicarbonyl compound **6**. Thus, although remarkable carbonyl anisotropic effects on the ¹H NMR spectra of **4** and **6** can be expected, it is not possible to compare the values obtained with the experimental chemical shift differences because only the 7-chloro/7-bromo derivatives (*cf.* Scheme 1) and not the parent compounds are experimentally available. Only the proton chemical shift of one of the H-2 protons in **6b,c** at 1.17 ppm may be employed as experimental proof of the strong shielding of the corresponding *syn* proton, subject to the carbonyl group anisotropic effects and for the existence of the preferred *syn* conformer in the *endo* configuration of these compounds as computed.

Conclusions

The conformational state, with respect to the five-membered ring inversion for the *exo* and *endo* configurations of the tetrahydrodicyclopentadiene derivatives **1–8**, was studied by variable-temperature dynamic NMR spectroscopy and by theoretical calculations. This dynamic process remains fast on the NMR timescale at 103 K and thus the conformational equilibria could not be frozen out. Computations provided ring-inversion barriers of 3.0–5.48 kcal mol⁻¹ and strongly one-sided conformational equilibria ($\Delta G° > 1.6$ kcal mol⁻¹) for the *anti* conformer of the *exo* isomers and, surprisingly, for the *syn* conformer of the *endo* isomers. TSNMRS as spatial magnetic properties (spatial NICS) of attached aryl (quinoxalyl) and carbonyl functional groups were successfully employed to prove the two conformations as the preferred conformers by agreement with the experimental chemical shift differences. This result was impressively corroborated by employing computed H,H-coupling constants for the same purpose.

Because of persistent strong reservations to qualify molecular response properties such as experimentally proven anisotropic effects of functional or aromatic groups on the ¹H chemical shifts of proximate protons by unobservable quantities like NICS,[24a] the results of this study can serve as definitive proof of TSNMRS (spatial NICS) to not only successfully assign the configuration and diastereoisomerism of structures,[2–14] but also the conformational state if the underlying dynamic process is fast on the NMR timescale. TSNMRS help visualize and quantify the anisotropic effects of functional groups in NMR spectra which can be measured experimentally and which can serve as the molecular response property of spatial NICS.

Experimental Section

All melting points were determined on a Boetius micro hostage microscope (Fa. Analytik Dresden). The IR spectra (KBr) were recorded with a Perkin Elmer FT-IR 1600 spectrometer (ν/cm^{-1}). The mass spectra were recorded on a Finnigan-MAT SSQ 710 (70 eV). ESI-MS spectra were obtained in positive ion mode using a Q-TOF$_{micro}$ mass spectrometer (Micromass Manchester, UK) which was equipped with an ESI source; analytes were injected using the syringe pump (Harvard Apparatur Ltd., Edenbridge, UK) at a flowing rate varying from 2 to 20 μL min^{-1} and the capillary voltage was set to 2.6 kV. Elemental compositions were determined by accurate measurements with deviations less than 10 ppm from the calculated values. Elemental analyses were performed on an autoanalyzer CHNS-932 (Fa. Leco instruments GmbH); reliable micromasses were obtained for all substances (C, H ± 0.3%). ^{1}H and ^{13}C NMR spectra were recorded on a Bruker Avance 500 or 300 MHz spectrometers using 5 mm probes operating at 500 and 300 MHz for ^{1}H, respectively, and 125 and 75 MHz for ^{13}C, respectively, and the low temperature NMR spectra on a Bruker AV 600 (at 600 and 150 MHz, respectively). Chemical shifts were determined relative to residual CHCl$_3$ (^{1}H, δ 7.27), internal CDCl$_3$ (^{13}C, δ 77.0), internal CD$_2$Cl$_2$ (^{13}C, δ 53.73) and are given in ppm downfield to TMS (for ^{1}H, ^{13}C). Analysis and assignment of the ^{1}H NMR data were supported by homonuclear (COSY) and heteronuclear (HSQC ^{13}C-^{1}H, HMBC ^{13}C-^{1}H) 2D correlation experiments. A solvent mixture of CD$_2$Cl$_2$, CHFCl$_2$, and CHF$_2$Cl in a ratio of 1 : 1 : 3 was used for the low temperature measurements. The probe temperature was calibrated by means of a thermocouple PT 100 inserted into a dummy tube. The low temperature measurements were estimated to be accurate to ±2 K. The chemical shifts difference $\Delta\nu_c$, Hz was computed at B3LYP/6-31G(d,p) level of theory and used to calculate k_c and the ring inversion barriers by the Eyring equation at T_c.

Preparation of 7-*syn*-chloro,9-*exo*-acetoxy-tetrahydro-*endo*-DCDP

To a stirred solution of 1,2-dihydro-*exo*-DCDP (0.50 mol, 67.1 g) in acetic acid (400 mL) *t*-butyl hypochlorite (0.50 mol, 54.3 g) was added dropwise at 20 °C. After removing the acetic acid under vacuum conditions, the residue was treated with diethyl ether, washed with NaOH (0.1 N) and water and dried with Na$_2$SO$_4$. The ether was removed by rotary evaporation and the residue was distilled under vacuum conditions, leaving colorless oil in 63% yield. n_D^{22}: 1.5068; Bp: 118–120 °C: IR (KBr, cm^{-1}): 726 (C–Cl), 1735 (C=O); ^{1}H NMR (ppm, CDCl$_3$): 4.89 (ddd, 1H, J = 1.30, 3.93, 7.60 Hz), 4.01 (tr, 1H, J = 1.1 Hz), 2.53–2.29 (m, 4H), 2.19 (ddd, 1H, J = 1.33, 7.64, 14.24 Hz), 2.09 (d, 1H, J = 2.66 Hz), 2.03 (s, 3H), 1.68–1.46 (m, 6H); ^{13}C NMR (ppm, CDCl$_3$): 171.00 (1C, C=O), 72.31 (1C, C–OR), 64.75 (1C, C–Cl), 51.92 (1C, CH), 47.74 (1C, CH), 41.81 (1C, CH), 41.32 (1C, CH), 31.14 (1C, CH$_2$), 28.20 (1C, CH$_2$), 27.31 (1C, CH$_2$), 26.64 (1C, CH$_2$), 21.34 (1C, CH$_3$); Anal. Calcd for C$_{12}$H$_{17}$ClO$_2$: C: 63.02, H: 7.49, found: C: 61.63, H: 7.06.

Preparation of 7-*syn*-chloro,9-*exo*-hydroxy-tetrahydro-*endo*-DCDP

7-*syn*- chloro,9-*exo*-acetoxy-tetrahydro-*endo*-DCDP (0.10 mol, 22.8 g) was treated with KOH (0.10 mol, 5.6 g) in 100 mL methanol

at 50 °C. After removing the methanol, the residue was dissolved in diethyl ether, washed with water and dried with Na$_2$SO$_4$. The ether was removed under reduced pressure, yielding crystals, which were recrystallized from *n*-hexane. The product was obtained as colorless needles in 93% yield. Mp. 39–41 °C; IR (KBr, cm^{-1}): 735 (C–Cl), 1060 (C–O), IR(CCl): 3586 (OH); ^{1}H NMR (ppm, CDCl$_3$): 4.08 (tr, 1H, J = 1.30 Hz), 3.96 (ddd, 1H, J = 1.52, 3.61, 7.74 Hz), 2.46–2.38 (m, 3H), 2.29 (m, 1H), 2.26 (ddd, 2H, J = 1.14, 7.74, 14.42 Hz), 1.88 (ddtr, 1H, J = 1.51, 4.13, 14.42 Hz), 1.63 (m, 2H), 1.52 (m, 4H); ^{13}C NMR (ppm, CDCl$_3$): 70.77 (1C, C–OH), 66.45 (1C, C–Cl), 54.06 (1C, CH), 47.84 (1C, CH), 41.50 (1C, CH), 40.80 (1C, CH), 34.87 (1C, CH$_2$), 27.97 (1C, CH$_2$), 27.44 (1C, CH$_2$), 26.79 (1C, CH$_2$); Anal. Calcd for C$_{10}$H$_{15}$ClO: C: 64.34, H: 8.10, found: C: 64.54, H: 7.61.

General procedure I – Oxidation of halogenohydrines to halogenoketones

To a stirred mixture of the adequate alcohol (0.25 mol) and diethylether (125 mL), 250 mL of a solution of Na$_2$Cr$_2$O$_7$ · 2H$_2$O (0.17 mol, 50 g) and H$_2$SO$_4$ (0.67 mol) in 250 mL water was added dropwise at 0 °C. The organic phase was separated, washed with NaOH (0.1 N) and water and dried with Na$_2$SO$_4$. The ether was removed by a rotary evaporator and the residue distilled under reduced pressure.

7-*syn*-chloro-tetrahydro-*endo*-DCDP-9-one (4b)

This compound was synthesized from 7-*syn*-chloro,9-*exo*-hydroxy-tetrahydro-*endo*-DCDP following the general procedure I. 7-*Syn*-chloro-tetrahydro-*endo*-DCDP-9-one was obtained as colourless oil in 76% yield.

Bp$_{1.5}$: 110–112 °C; n_D^{20}: 1,5278; IR (KBr, cm^{-1}): 745 (C–Cl), 1749 (C=O); Anal. Calcd for C$_{10}$H$_{13}$OCl: C: 65.04, H: 7.10, found: C: 65.00, H: 7.082; ^{1}H NMR (ppm, CDCl$_3$): 4.28 (ddd 1H), 2.72 (m, 4H), 2.58 (dd, ^{1}H, J = 18.53, 4.98 Hz), 2.16 (dd, 1H, J = 18.48, 2.58 Hz), 1.62 (m, 5H), 1.39 (m, 1H); MS (m/e, relative intensity): 185 [M^{35}Cl + 1]$^+$, 2), 120 (C$_9$H$_{12}$$^+$, 100), 107 (C$_8H_9$$^+$, 44), 79 (C$_6H_5$$^+$, 78).

7-*syn*-bromo-tetrahydro-*endo*-DCDP-9-one (4c)

This compound was synthesized from 7-*syn*-bromo,9-*exo*-hydroxy-tetrahydro-*endo*-DCDP following the general procedure I. 7-*Syn*-bromo-tetrahydro-*endo*-DCDP-9-one was obtained as colorless oil in 84% yield.

Bp$_{1.5}$: 132–133 °C; n_D^{20}: 1.5510; IR (KBr, cm^{-1}): 722 (C–Br), 1760 (C=O); MS: m/e (relative intensity): 229 (M^{79}Br + 1)$^+$, 14), 149 (C$_{10}$H$_{13}$O$^+$, 26), 107 (C$_8$H$_{11}$$^+$, 100), 79 (C$_6H_7$$^+$, 92); ^{1}H NMR (ppm, CDCl$_3$): 4.28 (m, 1H), 2.78–2.68, m, 4H), 2.61 (dd, 1H, J = 18.53, 4.53 Hz), 2.16 (dd, 1H, J = 18.53, 2.88 Hz), 1.79–1.70 (m, 1H), 1.70–1.50 (m, 4H), 1.39 (m, 1H); Anal. Calcd for C$_{10}$H$_{13}$OBr: C: 52.42, H: 5.72, found: C: 52.32, H: 5.791.

General procedure II – Oxidation of 7-*syn*-halogeno-tetrahydro-*endo*-DCPD-9-ones to 7-*syn*-halogeno-tetrahydro-*endo*-9,10-diones

A mixture of 7-*syn*-halogeno-tetrahydro-*endo*-DCPD-one (0.07 mol), selenedioxide (0.2 mol, 22.2 g) and 5 drops of water

in nitrobenzene (120 mL) was stirred for 5 h at 140 °C. Ether was then added, selen was removed by filtration and the solution was washed with NaOH (0.1 N) and water. After drying, both solvents were removed on a rotary evaporator. The residue was treated with ether and then purified by chromatography (Al$_2$O$_3$ neutral; pentane/ether, 1 : 5). The yellow residue obtained was recrystallized from acetone/hexane, 1 : 5.

7-*syn*-chloro-tetrahydro-*endo*-DCDP-9,10-dione (6b)

This compound was synthesized from 7-*syn*-chloro-tetrahydro-*endo*-DCDP-one **4b** following the general procedure II. 7-*syn*-chloro-tetrahydro-*endo*-DCDP-9,10-dione **6b** was obtained as yellow crystals in 61% yield. Mp: 109–110 °C; IR (KBr, cm^{-1}): 752 (C–Cl), 1755–1776 (C=O); ^{1}H NMR (600 MHz, CDCl$_3$): 4.55 (tr, 1H, J = 3.90 Hz), 3.29 (m, 2H), 3.02 (m, 2H), 1.68 (m, 2H), 1.63 (m, 1H), 1.46 (m, 2H), 1.17 (m, 1H); MS m/e (relative intensity): 198 (M^{35}Cl$^+$, 53), 237 (M^{37}Cl$^+$, 12), 107 (C$_{11}$H$_8$$^+$, 100); Anal. Calcd for C$_{10}$H$_{11}$O$_2$Cl: C:60.46; H:5.58, found: C: 60.59; H: 5.51.

7-*syn*-bromo-tetrahydro-*endo*-DCDP-9,10-dione (6c)

This compound was synthesized from 7-*syn*-bromo-tetrahydro-*endo*-DCDP-one **4c** following the general procedure II. 7-*Syn*-bromo-tetrahydro-*endo*-DCDP-9,10-dione **6c** was obtained as yellow crystals in 49% yield. Mp: 101 °C; IR(KBr, cm^{-1}): 752 (C–Br), 1752–1778 (C=O); ^{1}H NMR (600 MHz, CDCl$_3$): 4.39 (tr, 1H, J = 1.85 Hz), 3.34 (m, 2H), 3.02 (m, 2H) 1.7 (m, 2H), 1.64 (m, 1H), 1.47 (m, 2H), 1.18 (m, 1H); MS: m/e (relative intensity): 243 [M^{79}Br + 1]$^+$, 5), 107 (C$_8$H$_{11}$$^+$, 100), 79 (C$_6H_7$$^+$,72); Anal. Calcd for C$_{10}H_{11}O_2$Br: C: 49.41; H: 4.56, found: C: 49.53; H: 4.53.

General procedure III – Synthesis of quinoxaline derivatives 7 and 8 from the corresponding diketones 5 and 6, respectively

A mixture of tetrahydro-DCDP-9,10-dione (1.6 g, 0.01 mol), *o*-phenylendiamine (1.1 g, 0.01 mol) and benzene (50 mL) was stirred at room temperature. The solution was concentrated; purification of the residue by column chromatography and recrystallization from methanol.

Quinoxaline derivative 7a of tetrahydro-*exo*-DCDP-9,10-dione 5a

Anal. Calcd for C$_{16}$H$_{16}$N$_2$: C: 81.32; H: 6.82; N: 11.85, found: C:81.26; H: 6.99; N: 11.87. MS m/e (relative intensity): 236 (M$^+$, 100), 237 (M+1, 11), 168 (C$_{11}$H$_8$N$_2$, 90); ^{1}H NMR (600 MHz, CDCl$_3$): 7.96 (m, 2H); 7.63 (m, 2H); 3.29 (m, 2H); 2.27 (dtr, 2H, J = 12.4, 8.04 Hz); 2.17 (m, 1H); 2.07 (m, 2H); 1.98 (m, 1H); 1.94 (m, 1H); 1.51 (m, 1H); 1.29 (m, 2H); IR (cm^{-1}): 2860, 2879, 2951 (CH$_2$-valence), 1580 (C=C valence), 1510 (C=N valence), 1460 (CH$_2$ deform), 1363 (C–N valence).

Quinoxaline derivative 8a of tetrahydro-*endo*-DCDP-9,10-dione 6a

Anal. Calcd for C$_{16}$H$_{16}$N$_2$: C: 81.32; H: 6.82; N: 11.85, found: C:81.09; H: 6.93; N: 11.83. MS m/e (relative intensity): 236 (M$^+$, 100), 237 [M+1]$^+$, 11), 168 [C$_{11}$H$_8$N$_2$], 90); ^{1}H NMR (600 MHz, CDCl$_3$): 8.02 (m, 2H); 7.66 (m, 2H); 3.43 (dtr, 2H); 3.11 (m, 2H); 2.17 (m, 1H); 2.12 (m, 1H); 1.52 (m, 2H); 1.18 (m, 1H); 1.14 (m, 1H); −0.42 (m, 1H); IR (cm^{-1}): 2860, 2879, 2951 (CH$_2$-valence),

1580 (C=C valence), 1510 (C=N valence), 1460 (CH$_2$ deform), 1363 (C–N valence).

Notes and references

1 S. Klod and E. Kleinpeter, *J. Chem. Soc., Perkin Trans. 2*, 2001, 1893.
2 G. Tóth, J. Kovács, A. Lévai, A. Koch and E. Kleinpeter, *Magn. Reson. Chem.*, 2001, **39**, 251.
3 E. Kleinpeter and A. Holzberger, *Tetrahedron*, 2001, **57**, 6941.
4 A. Germer, S. Klod, M. G. Peter and E. Kleinpeter, *J. Mol. Model.*, 2002, **8**, 231.
5 S. Klod, A. Koch and E. Kleinpeter, *J. Chem. Soc., Perkin Trans. 2*, 2002, 1506.
6 J. Kovács, G. Tóth, A. Simon, A. Lévai, A. Koch and E. Kleinpeter, *Magn. Reson. Chem.*, 2003, **41**, 193.
7 E. Kleinpeter, S. Klod and W.-D. Rudorf, *J. Org. Chem.*, 2004, **69**, 4317.
8 E. Kleinpeter and S. Klod, *J. Am. Chem. Soc.*, 2004, **126**, 2231.
9 I. Szatmári, T. A. Martinek, L. Lázár, A. Koch, E. Kleinpeter, K. Neuvonen and F. Fülöp, *J. Org. Chem.*, 2004, **69**, 3645.
10 C. Ryppa, M. O. Senge, S. S. Hatscher, E. Kleinpeter, Ph. Wacker, U. Schilde and A. Wiehe, *Chem.–Eur. J.*, 2005, **11**, 3427.
11 E. Kleinpeter, A. Schulenburg, I. Zug and H. Hartmann, *J. Org. Chem.*, 2005, **70**, 6592.
12 E. Kleinpeter and A. Schulenburg, *J. Org. Chem.*, 2006, **71**, 3869.
13 M. Heydenreich, A. Koch, S. Klod, I. Szatmári, F. Fülöp and E. Kleinpeter, *Tetrahedron*, 2006, **62**, 11081.
14 E. Kleinpeter, A. Koch, H. S. Sahoo and D. K. Chand, *Tetrahedron*, 2008, **64**, 5044.
15 E. Kleinpeter, A. Koch and P. R. Seidl, *J. Phys. Chem. A*, 2008, **112**, 4989.
16 E. Kleinpeter, I. Szatmári, L. Lázár, A. Koch, M. Heydenreich and F. Fülöp, *Tetrahedron*, 2009, **65**, 8021.
17 E. Kleinpeter, S. Klod and A. Koch, *THEOCHEM*, 2007, **811**, 45 and references therein.
18 E. Kleinpeter, A. Holzberger and Ph. Wacker, *J. Org. Chem.*, 2008, **73**, 56.
19 E. Kleinpeter and A. Koch, *J. Phys. Chem. A*, 2010, **114**, 5928.
20 B. A. Shainyan, A. Fettke and E. Kleinpeter, *J. Phys. Chem. A*, 2008, **112**, 10895.
21 E. Kleinpeter, A. Koch, H. S. Sahoo and D. K. Chand, *Tetrahedron*, 2008, **64**, 5044.
22 (*a*) H. Fallah-Bagher-Shaidaei, C. S. Wannere, C. Corminboeuf, R. Puchta and P. von Ragué Schleyer, *Org. Lett.*, 2006, **8**, 863; (*b*) C. Corminboeuf, T. Heine, G. Seifert, P. von Ragué Schleyer and J. Weber, *Phys. Chem. Chem. Phys.*, 2004, **6**, 273.
23 A. Stanger, *Chem.–Eur. J.*, 2006, **12**, 2745.
24 (*a*) P. Lazzeretti, *Phys. Chem. Chem. Phys.*, 2004, **6**, 217; (*b*) St. Pelloni, P. Lazzeretti and R. Zanasi, *J. Phys. Chem. A*, 2007, **111**, 8163; (*c*) A. Stanger, *Chem. Commun.*, 2009, 1939.
25 Ch. A. Hunter and M. J. Paker, *Chem.–Eur. J.*, 1999, **5**, 1891.
26 M. A. McCoy and D. F. Wyss, *J. Am. Chem. Soc.*, 2002, **124**, 11758.
27 M. Cioffi, Ch. A. Hunter, M. J. Packer, M. J. Pandya and M. P. Williamson, *J. Biomol. NMR*, 2009, **43**, 11.
28 I. Alkorta and J. Elguero, *New J. Chem.*, 1998, **22**, 381.
29 (*a*) N. H. Martin, N. W. Allen III, K. D. Moore and L. Vo, *THEOCHEM*, 1989, **454**, 161; (*b*) N. H. Martin, N. W. Allen III, E. K. Minga, S. T. Ingrassia and J. D. Brown, *Proceedings of ACS Symposium, Modeling NMR Chemical Shifts: Gaining insight into Structure and Environment*, ACS Press, Washington, 1999.
30 (*a*) J. S. Waugh and R. W. Fessenden, *J. Am. Chem. Soc.*, 1957, **79**, 846; (*b*) C. E. Johnson and F. A. Bovey, *J. Chem. Phys.*, 1958, **29**, 1012; (*c*) N. Jonathan, S. Gordon and B. P. Dailey, *J. Chem. Phys.*, 1962, **36**, 2443; (*d*) M. Barfield, D. M. Grant and D. Ikenberry, *J. Am. Chem. Soc.*, 1975, **97**, 6956; (*e*) A. Agarwal, J. A. Barnes, J. L. Fletcher, M. J. McGlinchey and B. G. Saver, *Can. J. Chem.*, 1977, **55**, 2575; (*f*) C. W. Haigh and R. B. Mallion, *Progress in NMR Spectroscopy*, Pergamon Press, Ltd., New York, 1980, Vol. 13, pp 303.

1110 | *Org. Biomol. Chem.*, 2011, **9**, 1098–1111

This journal is © The Royal Society of Chemistry 2011

31 C. W. Haigh and R. B. Mallion, *Mol. Phys.*, 1971, **22**, 955.
32 (*a*) C. W. Haigh and R. B. Mallion, *Org. Magn. Reson.*, 1972, **4**, 203; (*b*) B. P. Dailey, *J. Chem. Phys.*, 1964, **41**, 2304.
33 (*a*) P. Wilder, Jr., C. F. Culberson and G. T. Youngblood, *J. Am. Chem. Soc.*, 1959, **81**, 655; (*b*) G. T. Youngblood and P. Wilder, Jr., *J. Am. Chem. Soc.*, 1956, **78**, 5706.
34 (*a*) I. H. Witt and C. S. Hamilton, *J. Am. Chem. Soc.*, 1945, **67**, 1178; (*b*) G. T. Youngblood and P. Wilder, Jr., *J. Org. Chem.*, 1956, **21**, 1436; (*c*) H. C. Brown, I. Rothberg and D. L. Vander Jagt, *J. Org. Chem.*, 1972, **37**, 4098; (*d*) S. J. Cristol, W. K. Seifert and S. B. Soloway, *J. Am. Chem. Soc.*, 1960, **82**, 2351.
35 H. A. Bruson and T. W. Riener, *J. Am. Chem. Soc.*, 1945, **67**, 723.
36 E. Kleinpeter, H. Kühn and M. Mühlstädt, *Org. Magn. Reson.*, 1976, **8**, 261.
37 (*a*) E. Kleinpeter, H. Kühn and M. Mühlstädt, *Org. Magn. Reson.*, 1976, **8**, 279; (*b*) E. Kleinpeter, H. Kühn, M. Mühlstädt, H. Jancke and D. Zeigan, *J. Prakt. Chem.*, 1982, **324**, 609; (*c*) E. Kleinpeter, H. Kühn, M. Mühlstädt and K. Pihlaja, *Finn. Chem. Lett.*, 1982, 25.
38 M. J. Frisch, G. W. Trucks, H. B. Schlegel, G. E. Scuseria, M. A. Robb, J. R. Cheeseman, J. A. Montgomery, Jr., T. Vreven, K. N. Kudin, J. C. Burant, J. M. Millam, S. S. Iyengar, J. Tomasi, V. Barone, B. Mennucci, M. Cossi, G. Scalmani, N. Rega, G. A. Petersson, H. Nakatsuji, M. Hada, M. Ehara, K. Toyota, R. Fukuda, J. Hasegawa, M. Ishida, T. Nakajima, Y. Honda, O. Kitao, H. Nakai, M. Klene, X. Li, J. E. Knox, H. P. Hratchian, J. B. Cross, V. Bakken, C. Adamo, J. Jaramillo, R. Gomperts, R. E. Stratmann, O. Yazyev, A. J. Austin, R. Cammi, C. Pomelli, J. Ochterski, P. Y. Ayala, K. Morokuma, G. A. Voth, P. Salvador, J. J. Dannenberg, V. G. Zakrzewski, S. Dapprich, A. D. Daniels, M. C. Strain, O. Farkas, D. K. Malick, A. D. Rabuck, K. Raghavachari, J. B. Foresman, J. V. Ortiz, Q. Cui, A. G. Baboul, S. Clifford, J. Cioslowski, B. B. Stefanov, G. Liu, A. Liashenko, P. Piskorz, I. Komaromi, R. L. Martin, D. J. Fox, T. Keith, M. A. Al-Laham, C. Y. Peng, A. Nanayakkara, M. Challacombe, P. M. W. Gill, B. G. Johnson, W. Chen, M. W. Wong, C. Gonzalez and J. A. Pople, *GAUSSIAN 03 (Revision C.02)*, Gaussian, Inc., Wallingford, CT, 2004.
39 A. D. Becke, *J. Chem. Phys.*, 1993, **98**, 5648.
40 C. Lee, W. Yang and R. G. Parr, *Phys. Rev. B:*, 1988, **37**, 785.
41 R. Ditchfield, W. J. Hehre and J. A. Pople, *J. Chem. Phys.*, 1971, **54**, 724.
42 R. Ditchfield, *Mol. Phys.*, 1974, **27**, 789.
43 S. Miertus and J. Tomasi, *Chem. Phys.*, 1982, **65**, 239.
44 P. von Ragué Schleyer, M. Manoharan, Z. X. Wang, B. Kiran, Y. Jiao, R. Puchta and N. J. R. von Hommes, *Org. Lett.*, 2001, **3**, 2465.
45 SYBYL 7.3 Tripos Inc. 1699 South Hanley Road, St. Louis, Missouri 63144, USA, 2007.
46 K. Pihlaja and E. Kleinpeter, Carbon-13 NMR Chemical Shifts in Structural and Stereochemical Analysis, in *Methods in Stereochemical Analysis*, ed. A. P. Marchand, VCH, New York, 1994.
47 A. E. Aliev and D. Courtier-Murias, *J. Phys. Chem. B*, 2007, **111**, 14034.
48 PERCH solutions Ltd. Kuopio, Finland. R. Laatikainen, *J. Magn. Reson.*, 1991, **92**, 1; R. Laatikainen, *QCMP100. MLDC8 QCPE Bull.*, 1992, **12**, 23; R. Laatikainen, M. Niemitz, U. Weber, J. Sundelin, T. Hassinen and J. Vepsäläinen, *J. Magn. Reson.*, 1996, **A120**, 1; R. Laatikainen, M. Niemitz, W. J. Malaisse, M. Biesemans and R. Willem, *Magn. Reson. Med.*, 1996, **36**, 359.